JOURNAL OF INFORMATION AND COMMUNICATION TECHNOLOGY
http://e-journal.uum.edu.my/index.php/jict

How to cite this article:
Abdullah, S. A., & Jumaat, A. K. (2022). Selective image segmentation models using three distance functions. *Journal of Information and Communication Technology, 21*(1), 95-116. https://doi.org/10.32890/jict2022.21.1.5

Selective Image Segmentation Models Using Three Distance Functions

[1]Siti Aminah Abdullah & [*2]Abdul Kadir Jumaat
[1,2]Faculty of Computer and Mathematical Sciences,
Universiti Teknologi MARA, Shah Alam, Malaysia

[1]2020534771@student.uitm.edu.my
[2]abdulkadir@tmsk.uitm.edu.my
[*]Corresponding author

Received: 10/4/2021 Revised: 25/7/2021 Accepted: 2/8/2021 Published: 11/11/2021

ABSTRACT

Image segmentation can be defined as partitioning an image that contains multiple segments of meaningful parts for further processing. Global segmentation is concerned with segmenting the whole object of an observed image. Meanwhile, the selective segmentation model is focused on segmenting a specific object required to be extracted. The Convex Distance Selective Segmentation (CDSS) model, which uses the Euclidean distance function as the fitting term, was proposed in 2015. However, the Euclidean distance function takes time to compute. This paper proposed the reformulation of the CDSS minimization problem by changing the fitting term with three popular distance functions, namely Chessboard, City Block, and Quasi-Euclidean. The proposed models were $CDSS_{NEW1}$, $CDSS_{NEW2}$, and $CDSS_{NEW3}$, which applied the Chessboard, City Block, and

Quasi-Euclidean distance functions, respectively. In this study, the Euler-Lagrange (EL) equations of the proposed models were derived and solved using the Additive Operator Splitting method. Then, MATLAB coding was developed to implement the proposed models. The accuracy of the segmented image was evaluated using the Jaccard and Dice Similarity Coefficients. The execution time was recorded to measure the efficiency of the models. Numerical results showed that the proposed $CDSS_{NEW1}$ model based on the Chessboard distance function could segment specific objects successfully for all grayscale images with the fastest execution time as compared to other models.

Keywords: Active contour, convex distance selective segmentation, convex functional, selective variational image segmentation.

INTRODUCTION

Image segmentation is a procedure of dividing a digital image that is comprised of common features and properties and shares certain characteristics into multiple segments (Kumar et al., 2014). Image segmentation is necessary to analyze and segmentize an image into various parts that may be useful for basic applications such as in the fields of robotics, image analysis, medical diagnosis, and object detection (Saini & Arora, 2014). Two segmentation techniques are available, i.e., based on discontinuity and similarity (Saini & Arora, 2014).

According to Zuva et al. (2011), the discontinuity property of pixel-based segmentation methods is classified as edge-based techniques. Generally, edge detection techniques are used to find discontinuities in a gray level image. The techniques that are useful for shape boundary recognition (Othman et al., 2016) can be implemented using edge detection operators, such as Prewitt, Sobel, Roberts, Canny, and Test operators (Saini & Arora, 2014).

Meanwhile, the segmentation method based on similarity criteria is considered as a region-based technique. It divides an entire image into sub-regions or clusters, and similar or homogeneous areas of connected pixels. Each pixel in a region can share similar characteristics such as color, intensity, or texture. If a similarity property is met, the pixel can be designated as one or more of its neighbors in the cluster, resulting

in fewer regions and a bigger image (Khan & Ravi, 2013). Several similarity-based techniques that are commonly used are simple intensity thresholding (Hadhoud et al., 2005), watershed approaches (Beucher, 1990), clustering-based segmentation (Shihab, 2000), and variational methods (Jumaat & Chen, 2020).

The discontinuity approaches associated with edge-based techniques are low-level segmentation techniques that may incorrectly identify the region or boundary of an object due to the distraction of noise in an image (Mclnerny & Terzopoulos, 1996). Meanwhile, of all the similarity techniques mentioned earlier, the variational methods have been proven to be very efficient for image segmentation as compared to other models (Jumaat & Chen, 2017). Therefore, based on these facts, this research focuses on variational approaches to segment images.

Several variational methods have been proven to be efficient with different properties of a set of images and offer high-quality processing capabilities for imaging (Dobrosotskaya & Weihong, 2017; Kaur & Kaur, 2014; Khan, 2014). According to Spencer and Chen (2015), variational-based approaches are connected to stochastic-based approaches that analyze the observed original image in the discrete form of a continuous domain. Next, an appropriate minimizing functional problem related to original image processing problems needs to be solved. According to Yearwood (2018), to obtain minimum or maximum optimality, variational methods use the calculus of variations to optimize the cost function. The methods introduced by Kass et al. (1988), Mumford and Shah (1989), Perona and Malik (1990), Caselles et al. (1997), Chan and Vese (2001), Gout et al. (2005), Chan et al. (2006), Rada and Chen (2011), Brown et al. (2012), Getreuer (2012), Spencer and Chen (2015), Bastan et al. (2017), Jumaat and Chen (2019), and Burrows et al. (2020), as well as other variational methods, were proposed to improve the efficiency of segmentation results.

Global and selective segmentation methods are two different approaches used in variational image segmentation. The methods concerned with the segmentation of all contour objects in observed images are classified as the global segmentation approach. Interestingly, the models proposed by Mumford and Shah (1989), Chan and Vese (2001), Gout et al. (2005), Li et al. (2011), Yang and

Wu (2012), Mandal et al. (2016), and Wei et al. (2017) are examples of the global segmentation model. However, according to Rada and Chen (2013), the global segmentation techniques cannot be applied to extract only a specific object in a given image. To do so, a more appropriate approach to accomplish the task is by using selective segmentation techniques.

The selective segmentation is concerned with the segmentation of particular regions and features of the observed image (Ali et al., 2018). Some effective selective models have been proposed such as by Badshah and Chen (2010), Li et al. (2011), Rada and Chen (2013), and the Convex Distance Selective Segmentation (CDSS) model by Spencer and Chen (2015).

The numerical experiment conducted by Spencer and Chen (2015) demonstrated that the CDSS model performed better than other existing models. In addition, the CDSS model is effective, as the convexity could find the global minimizer and improve the reliability of the solution (Jumaat & Chen, 2019). The CDSS model uses the Euclidean distance function in its functional minimization. According to Lee and Horng (1996), finding the Euclidean distance transform is time-consuming.

The distance functions commonly used are Euclidean, City Block, and Chessboard (Chen et al., 2004). The Euclidean distance between two pixels is a simple straight-line distance, and the Euclidean norm is used to evaluate it (Felzenszwalb & Huttenlocher, 2012). City Block, also known as Manhattan distance, measures the path between four connected pixels in a neighborhood. This is a fundamental operation in computer vision, pattern recognition, and robotics.

Meanwhile, the Chessboard distance, also known as the Chebyshev distance, calculates the path between pixels using eight connected neighbors. The distance is defined on a vector space as the maximum differences of two vectors in any coordinate dimension. On the other hand, the total Euclidean distance along the vertical, horizontal, and diagonal line segments is measured by the Quasi-Euclidean metric.

Chen et al. (2004) demonstrated that different distance transforms produce different computation and segmentation results. Based on the watershed segmentation results, the Euclidean distance transform and City block distance transform performed poorly as compared to the Chessboard distance transform. Furthermore, the errors produced by

the Euclidean and City Block distance functions are higher than those generated by the Chessboard method in detecting objects in a given image.

Since the different distance transforms may yield different results in image segmentation, this study is interested in investigating the effect of modifying the CDSS model with different distance transforms. Three distance transforms are used in this study, i.e., Chessboard, City Block, and Quasi-Euclidean. By this modification, a certain degree of improvement is expected in the computational speed and accuracy of the segmentation results.

The next part of this paper provides a brief review of the study, which is then followed by the formulations of the proposed convex and selective models. The experimental results of existing and proposed models are then presented.

REVIEW ON RELATED MODELS

Based on previous research, several variational-based segmentation models for both global and selective segmentations exist. The two existing segmentation models related to the new proposed model are discussed below, i.e., the Chan and Vese (2001) and Spencer and Chen (2015) models.

The Chan and Vese (2001) Model

The Active Contour Without Edges variational mathematical formulation was developed by Chan and Vese (2001) for image segmentation. The Chan and Vese (2001) model is abbreviated as the CV model in this study. It was formulated based on the piecewise constant two-phase functional introduced by Mumford and Shah (1989). An image is assumed as $z = z(x, y)$. In their model, the assumption made was that image z was designed by two main regions. The unknown contour, Γ, separated the regions. Inside the curve or contour Γ, the region Ω_1 was assumed to represent the specific object with the unknown value, c_1. Outside the curve Γ, the image intensity was approximated by the unknown value c_2 in $\Omega_2 = \Omega / \Omega_1$. Then, using $\Omega = \Omega_1 \cup \Omega_2$, the CV model minimized the following Equation 1:

$$\min_{\Gamma, c_1, c_2} \left\{ CV(\Gamma, c_1, c_2) = \mu \text{ length}(\Gamma) + \lambda_1 \int_{\Omega_1} (z - c_1)^2 \, dxdy + \lambda_2 \int_{\Omega_2} (z - c_2)^2 \, dxdy. \right\} \quad (1)$$

Based on Equation 1, the unknown constants c_1 and c_2 are considered as the approximately piecewise constant intensities of the mean values of z inside and outside the variable contour Γ,. Meanwhile, parameters μ, λ_1, and λ_2, which are non-negative parameters, represent the weights for the regularizing term and fitting term, respectively. The level set method was applied by following the idea introduced by Osher et al. (1988). The regularized functions H and δ are defined by the following Equation 2:

$$\begin{aligned} H\left(\phi(x,y)\right) &= \tfrac{1}{2}\left[1+\tfrac{\phi}{\varepsilon}+\tfrac{1}{\pi}\sin\left(\pi\phi/\varepsilon\right)\right], \\ \delta\left(\phi(x,y)\right) &= \tfrac{1}{2\varepsilon}\left[1+\cos\left(\tfrac{\pi\phi}{\varepsilon}\right)\right], \end{aligned} \tag{2}$$

where ε is a constant used to avoid the values of $H\left(\phi(x,y)\right)$ and $\delta\left(\phi(x,y)\right)$ tends to be zero, leading to the failure of an object to be extracted if it is far from the initial contour. Thus, Equation 1 is modified as in the following Equation 3:

$$\left.\begin{aligned} \left(\phi, c_1, c_2\right) = \mu\int_\Omega \left|\nabla H\left(\phi\right)\right| dxdy \;+\; \lambda_1\int_\Omega \left(z-c_1\right)^2 H\left(\phi\right) dxdy \\ +\; \lambda_2\int_\Omega \left(z-c_2\right)^2 \left(1-H\left(\phi\right)\right) dxdy. \end{aligned}\right\} \tag{3}$$

The function ϕ was fixed. Then, Equation 3 was minimized with respect to c_1 and c_2 that yield the following Equation 4:

$$\begin{aligned} c_1\left(\phi\right) &= \int_\Omega z(x,y) H\left(\phi(x,y)\right) d\Omega \,/\, \int_\Omega H\left(\phi(x,y)\right) d\Omega \\ c_2 &= \int_\Omega z(x,y)\left(1-H\left(\phi(x,y)\right)\right) d\Omega \,/\, \int_\Omega H\left(\phi(x,y)\right) d\Omega\,. \end{aligned} \tag{4}$$

Fixing c_1 and c_2 as constants in $CV\left(\phi, c_1, c_2\right)$ leads to the following Equation 5 for ϕ:

$$\begin{cases} \mu\delta\left(\phi\right)\nabla.\left(\dfrac{\nabla\phi}{|\nabla\phi|}\right) - \lambda_1\delta\left(\phi\right)\left(z-c_1\right)^2 + \lambda_2\delta\left(\phi\right)\left(z-c_2\right)^2 = 0 \;\; in\ \Omega, \\ \dfrac{\delta\left(\phi\right)}{|\nabla\phi|}\dfrac{\partial u}{\partial\vec{n}} = 0 \qquad\qquad\qquad\qquad\qquad\qquad on\ \partial\Omega. \end{cases} \tag{5}$$

where $\nabla\phi$ represents the gradient of the level set function ϕ. Equation 5 is called as the Euler-Lagrange (EL) equation, which was solved using a finite difference method.

The Spencer and Chen (2015) Model

A new formulation for the selective model was developed by Spencer and Chen (2015), termed the Distance Selective Segmentation (DSS) model. This two-phase model was based on the piecewise constant functional introduced by Chan and Vese (2001). Let be a $z(x,y)$ grayscale image. The marker set was given as $A=\{w_i=(x_i^*,y_i^*)\in\Omega, 1\le i\le n_1\}$ with $n_1(\ge 3)$ marker points. The polygon R would be constructed using set A that linked up the markers. In the model, the normalized Euclidean distance $P_d(x,y)$ of each point $(x,y)\in\Omega$ from its nearest point in the polygon, made up of $(x_p,y_p)\in P$, constructed from user input set, A was introduced. The function $P_d(x,y)$ is defined by the following Equation 6:

$$P_d(x,y)=\frac{P_0(x,y)}{\|P_0\|_{L\infty}} \tag{6}$$

where $P_0(x,y)=\sqrt{(x-x_p)^2+(y-y_p)^2}$. Then, the DSS formulation is given as the following Equation 7:

$$\begin{aligned} DSS(\Gamma,c_1,c_2)=\mu|\Gamma|+\theta\int_{in(\Gamma)}P_d(x,y)\,d\Omega \\ +\lambda\int_{in(\Gamma)}(z-c_1)^2\,d\Omega+\lambda\int_{out(\Gamma)}(z-c_2)^2\,d\Omega\,. \end{aligned} \tag{7}$$

In the level set representation, Equation 7 can be written as the following Equation 8:

$$\begin{aligned} \min_{\phi,c_1,c_2}\{DSS(\phi,c_1,c_2)=\mu\int_\Omega\delta(\phi)|\nabla\phi|\,d\Omega+\theta\int_\Omega H(\phi)P_d\,d\Omega \\ +\lambda\int_\Omega H(\phi)(z-c_1)^2\,d\Omega+\lambda\int_\Omega(1-H(\phi))(z-c_2)^2\,d\Omega\}, \end{aligned} \tag{8}$$

for non-negative parameters θ, λ and μ. Here, ϕ is the area parameter that controls the weight of the distance fitting term, the parameter λ controls the region fitting term, while the parameter μ controls the length of the generated curve. Normally, $\mu=\lambda=1$. It was suggested that the chosen value of θ was different for each image and the value depended on the targeted object. In practice, a small was θ needed for a simple image, while a large θ was suitable for a low contrast image close to the neighboring area. The convex formulation was introduced by reformulating Equation 8 by taking the adjustment about the Heaviside function as $H(\phi)\to u\in[0,1]$. Thus, the new function was known as the Convex Distance Selective Segmentation (CDSS), defined as an unconstrained minimization problem as in the following Equation 9:

$$\min_{u}\{CDSS(u,c_1,c_2)=\mu\int_{\Omega}|\nabla u|\,d\Omega+\int_{\Omega}ru\,d\Omega+\theta\int_{\Omega}P_d u d\Omega+\alpha\int_{\Omega}v(u)d\Omega\}. \quad (9)$$

where $r=(z-c_1)^2-(z-c_2)^2$. The regularized version of penalty function, *v*, is defined by the following Equation 10:

$$v(u)=H\left(\sqrt{(2u-1)^2+\varepsilon}-1\right)\left[\sqrt{(2u-1)^2+\varepsilon}-1\right], \quad (10)$$

where $H(x)=\frac{1}{2}\left(1+\frac{2}{\pi}\arctan\left(\frac{x}{\varepsilon}\right)\right)$. Then, the following Euler-Lagrange partial differential equation (PDE) for *u* is defined by the following Equation 11:

$$\begin{cases}\mu\nabla.\left(\dfrac{\nabla u}{|\nabla u|}\right)-\lambda r-\theta P_d-\alpha v'=0 & \text{in } \Omega\\ \dfrac{\partial u}{\partial n}=0 & \text{on } \partial\Omega\end{cases} \quad (11)$$

Here, the parameter α is a weightage parameter for the penalty term, v. The CDSS functional problem used one of the most common distance functions, the Euclidean distance function, in its function. The Euler-Lagrange Equation 11 was solved by using the Additive Operator Splitting (AOS_2) method introduced by Spencer and Chen in 2015.

THE PROPOSED MODELS

This research aimed to modify the CDSS model by substituting the distance function, $P_d(x,y)$, with different distance functions, i.e., Chessboard, City Block, and Quasi-Euclidean, which is generally in the form of the following Equation 12:

$$\min_{u} CDSS_{NEW}(u,c_1,c_2). \quad (12)$$

A given image $z=z(x,y)$ is indicated with image domain $\Omega\subset\mathbb{R}^2$. Assume the availability of $n_1(\geq 3)$ points inside the targeted object that form a marker set $B=\left\{w_i=(x_i^*,y_i^*)\in\Omega, 1\leq i\leq n_1\right\}$ that defines a polygon. The geometrical points in B defined an initial polygonal contour and polygon Ƥ would be constructed by connecting the markers using set B. The function $P_C(x,y)$ was denoted as the Chessboard distance, $P_{CB}(x,y)$ as the City Block distance, and $P_{QE}(x,y)$ as the Quasi-Euclidean of each point $(x,y)\in\Omega$ from its nearest point $(x_p,y_p)\in$ Ƥ, constructed from user input set B. The distance functions $P_C(x,y)$, $P_{CB}(x,y)$, and $P_{QE}(x,y)$ are defined by the following Equations 13, 14, and 15, respectively:

i) Chessboard distance function,

$$P_C(x,y) = \max\left(|x_1 - x_p|, |y_1 - y_p|\right) \quad (13)$$

ii) City Block distance function,

$$P_{CB}(x,y) = |x_1 - x_p|, |y_1 - y_p| \quad (14)$$

iii) Quasi-Euclidean distance function,

$$P_{QE}(x,y) = \begin{cases} |x_1 - x_2| + (\sqrt{2}-1)|y_1 - y_2| & , \ |x_1 - x_2| > |y_1 - y_2| \\ (\sqrt{2}-1)|x_1 - x_2| + |y_1 - y_2| & , \ \text{otherwise.} \end{cases} \quad (15)$$

Based on the general form of the modified model in Equation 12 and the related distance functions above, this study proposed three new variants of modified CDSS concerning three different distance functions as follows:

i) let $CDSS_{NEW} = CDSS_{NEW1}$, which represents a modified CDSS by using the Chessboard distance function. The first modified model is defined by the following Equation 16:

$$\min_u \{CDSS_{NEW1}(u, c_1, c_2) = \mu \int_\Omega |\nabla u| \, d\Omega + \lambda \int_\Omega ru \, d\Omega + \theta \int_\Omega P_C u d\Omega + \alpha \int_\Omega v(u) d\Omega\} \quad (16)$$

ii) let $CDSS_{NEW} = CDSS_{NEW2}$, which is a modified CDSS by using the City Block distance function. The second modified model is defined by the following Equation 17:

$$\min_u \{CDSS_{NEW2}(u, c_1, c_2) = \mu \int_\Omega |\nabla u| \, d\Omega + \lambda \int_\Omega ru \, d\Omega + \theta \int_\Omega P_{CB} u d\Omega + \alpha \int_\Omega v(u) d\Omega\} \quad (17)$$

iii) let $CDSS_{NEW} = CDSS_{NEW3}$. The third modified model is defined by the following Equation 18:

$$\min_u \{CDSS_{NEW3}(u, c_1, c_2) = \mu \int_\Omega |\nabla u| \, d\Omega + \lambda \int_\Omega ru \, d\Omega + \theta \int_\Omega P_{QE} u d\Omega + \alpha \int_\Omega v(u) d\Omega\} \quad (18)$$

which represents a modified CDSS using the Quasi-Euclidean distance function. Here, $r = (z - c_1)^2 - (z - c_2)^2$. The function $v(u)$ is defined similar to Equation 10.

The modified models above were minimized using the Calculus of Variation by deriving their Euler-Lagrange PDE. A short derivation of the Euler-Lagrange equation with respect to for this study is shown below. The derivation of the Euler-Lagrange equation for Equation 16 is only demonstrated, as the derivations of Equations 17 and 18 are similar.

From Equation 16, denote $I_1(u) = |\nabla u| = \sqrt{u_x^2 + u_y^2} = (u_x^2 + u_y^2)^{1/2}$, $I_2(u) = ru$, $I_3(u) = P_C u$, and $I_4(u) = v(u)$.

Evidently, $I_1|u + \bar{\varepsilon}\phi| = |\nabla(u + \bar{\varepsilon}\phi)| = \sqrt{(u_x + \bar{\varepsilon}\phi_x)^2 + (u_y + \bar{\varepsilon}\phi_y)^2}$, where $\bar{\varepsilon}$ is a real parameter that is restricted to some intervals around 0 and ϕ is a test function. The derivative for I_1 with respect to $\bar{\varepsilon}$ is given as:

$$\frac{d}{d\bar{\varepsilon}}|\nabla(u + \bar{\varepsilon}\phi)| = \frac{d}{d\bar{\varepsilon}}\sqrt{(u_x + \bar{\varepsilon}\phi_x)^2 + (u_y + \bar{\varepsilon}\phi_y)^2}$$

$$= \frac{1}{2}\left[(u_x + \bar{\varepsilon}\phi_x)^2 + (u_y + \bar{\varepsilon}\phi_y)^2\right]^{-\frac{1}{2}} \cdot \left[2(u_x + \bar{\varepsilon}\phi_x)\phi_x + 2(u_y + \bar{\varepsilon}\phi_y)\phi_y\right]$$

At $\bar{\varepsilon} = 0$, $\frac{d}{d\bar{\varepsilon}}|\nabla(u + \bar{\varepsilon}\phi)| = \frac{u_x\phi_x + u_y\phi_y}{\left[u_x^2 + u_y^2\right]^{\frac{1}{2}}} = \frac{\nabla u.\nabla\phi}{|\nabla u|}$. From this point, the Taylor expansion was applied. For example, consider the function $f(a) = (x + ac_1)^2 + (y + ac_2)^2]^p$ where $p \neq 0$. The derivative with respect to a is:

$$\frac{d}{da}(f(a)) = f'(a) = p[(x + ac_1)^2 + (y + ac_2)^2]^{p-1}\left(2(x + ac_1)c_1 + 2(y + ac_2)c_2\right)$$

and at $a=0$ gives $f'(0) = \left(2(x)c_1 + 2(y)c_2\right) = p\frac{(2xc_1 + 2yc_2)}{[x^2 + y^2]^{p-1}}$. Then, the Taylor expansion at $a=0$ is defined by the following Equation 19:

$$f(a) = f(0) + f'(a)a + O(a^2) = (x^2 + y^2)^P + p\frac{(2xc_1 + 2yc_2)}{(x^2 + y^2)^{1-p}}a + O(a^2). \quad (19)$$

Therefore, by applying the Taylor expansion in Equation 19 at $\bar{\varepsilon} = 0$, the term I_1 can be extended as follows:

$$I_1|u + \bar{\varepsilon}\phi| = |\nabla(u + \bar{\varepsilon}\phi)| = \sqrt{(u_x + \bar{\varepsilon}\phi_x)^2 + (u_y + \bar{\varepsilon}\phi_y)^2} = |\nabla u| + \frac{\nabla u.\nabla\phi}{|\nabla u|}\bar{\varepsilon} + O(\bar{\varepsilon}^2)$$

Next, compute the derivative for I_2 with respect to $\bar{\varepsilon}$ as follows:

$$\frac{d}{d\bar{\varepsilon}}(u + \bar{\varepsilon}\phi)r = r\phi,$$

At $\bar{\varepsilon} = 0$, $\frac{d}{d\bar{\varepsilon}}(r(u + \bar{\varepsilon}\phi) = r\phi$. Therefore, by applying the Taylor series expansion in Equation 19 at $\bar{\varepsilon} = 0$, I_2 becomes:

$$r(u + \bar{\varepsilon}\phi) = ru + r\phi\bar{\varepsilon} + O(\bar{\varepsilon}^2)$$

For the function I_3, the derivative with respect to $\bar{\varepsilon}$ is as follows:

$$\frac{d}{d\bar{\varepsilon}}(u+\bar{\varepsilon}\phi)P_{C.} = P_C.\phi\,.$$

At $\bar{\varepsilon}=0$, $\frac{d}{d\bar{\varepsilon}}(P_C(u+\bar{\varepsilon}\phi) = P_C\cdot\phi$ After applying the Taylor expansion in Equation 19 at $\bar{\varepsilon}=0$, I_3 becomes:

$$P_C(u+\bar{\varepsilon}\phi) = P_C u + P_C\phi\bar{\varepsilon} + O(\bar{\varepsilon}^2)$$

Similarly, for function I_4 ,the derivative with respect to $\bar{\varepsilon}$ is given as:

$$\frac{d}{d\bar{\varepsilon}}(v(u+\bar{\varepsilon}\phi) = v'(u+\phi\bar{\varepsilon}).\phi$$

At $\bar{\varepsilon}=0$, $\frac{d}{d\bar{\varepsilon}}(v(u+\bar{\varepsilon}\phi) = v'(u).\phi$. Therefore, by applying the Taylor expansion in Equation 19 $\bar{\varepsilon}=0$, I_4 at becomes:

$$v(u+\bar{\varepsilon}\phi) = v(u) + v'(u)\phi\bar{\varepsilon} + O(\bar{\varepsilon}^2)$$

Now, compute the first variation of the functional $CDSS_{NEW1}$ of Equation 16 with respect to *u*. With any test function ϕ the first variation for $I(u) = I_1(u) + I_2(u) + I_3(u) + I_4(u)$ is given as:

$$\int_\Omega \frac{I(u+\bar{\varepsilon}\phi)-I(u)}{\bar{\varepsilon}} =$$

$$\frac{1}{\bar{\varepsilon}}\int_\Omega \left[\begin{array}{l}\mu\left[|\nabla u| + \frac{\nabla u.\nabla\phi}{|\nabla u|}\bar{\varepsilon} + O(\bar{\varepsilon}^2) - |\nabla u|\right] + \lambda\left[ru + r\phi\bar{\varepsilon} + O(\bar{\varepsilon}^2) - ru\right] + \\ \theta\left[P_C u + P_C\phi\bar{\varepsilon} + O(\bar{\varepsilon}^2) - P_C u\right] + \alpha\left[v(u) + v'(u)\phi\bar{\varepsilon} + O(\bar{\varepsilon}^2) - v(u)\right]\end{array}\right] d\Omega$$

This is simplified as:

$$\int_\Omega \frac{I(u+\bar{\varepsilon}\phi)-I(u)}{\bar{\varepsilon}} =$$

$$\int_\Omega \left[\mu\left[\frac{\nabla u.\nabla\phi}{|\nabla u|} + O(\bar{\varepsilon}^2)\right] + \lambda\left[r\phi + O(\bar{\varepsilon}^2)\right] + \theta\left[P_C\phi + O(\bar{\varepsilon}^2)\right] + \alpha\left[v'(u)\phi + O(\bar{\varepsilon}^2)\right]\right] d\Omega$$

Consequently, for any ϕ, $\lim_{\bar{\varepsilon}\to 0}\frac{I(u+\bar{\varepsilon}\phi)-I(u)}{\bar{\varepsilon}} = 0$. Hence,

$$\int_\Omega \frac{I(u+\bar{\varepsilon}\phi)-I(u)}{\bar{\varepsilon}} = \int_\Omega \left[\mu\frac{\nabla u.\nabla\phi}{|\nabla u|} + \lambda r\phi + \theta P_C\phi + \alpha v'(u)\phi\right] d\Omega = 0$$

Using Green's first identity as the following relation:

$$\int_\Omega \nabla\phi.\vec{\omega}\, d\Omega = \int_{d\Omega}\phi\vec{\omega}.\vec{\eta}\, ds - \int_\Omega \phi\nabla.\vec{\omega}\, d\Omega,$$

and by taking $\vec{\omega} = \frac{\nabla u}{|\nabla u|}$, the following is obtained:

$$\int_{\Omega} \nabla \phi . \vec{\omega} d\Omega = \int_{\Omega} \frac{\nabla u}{|\nabla u|} . \nabla \phi d\Omega = \int_{d\Omega} \phi . \frac{\nabla u}{|\nabla u|} . \vec{\eta} \, ds - \int_{\Omega} \nabla \cdot \frac{\nabla u}{|\nabla u|} \phi \, d\Omega$$

Therefore, by setting the boundary condition (Neumann Type) $\nabla u . \eta = 0$:

$$\int_{\Omega} \left[-\mu \nabla \cdot \frac{\nabla u}{|\nabla u|} \phi + \lambda r \phi + \theta P_C \phi + \alpha v'(u) \phi \right] d\Omega = 0$$

The integrand is zero if:

$$-\mu \nabla \cdot \frac{\nabla u}{|\nabla u|} \phi + \lambda r \phi + \theta P_C \phi + \alpha v'(u) \phi = 0$$

$$\Rightarrow \phi \left[-\mu \nabla \cdot \frac{\nabla u}{|\nabla u|} + \lambda r + \theta P_C + \alpha v'(u) \right] = 0$$

Therefore, for all test functions ϕ the Euler-Lagrange PDE with Neumann boundary condition for the proposed $CDSS_{NEW1}$ model in Equation 16 is defined by the following Equation 20:

$$-\mu \nabla \cdot \frac{\nabla u}{|\nabla u|} + \lambda r + \theta P_C + \alpha v'(u) = 0 \tag{20}$$

By similar processes, the Euler-Lagrange PDE for $CDSS_{NEW2}$ and $CDSS_{NEW3}$ is defined by Equations 21 and 22 as follows:

$$-\mu \nabla \cdot \frac{\nabla u}{|\nabla u|} + \lambda r + \theta P_{CB} + \alpha v'(u) = 0 \tag{21}$$

$$-\mu \nabla \cdot \frac{\nabla u}{|\nabla u|} + \lambda r + \theta P_{QE} + \alpha v'(u) = 0 \tag{22}$$

Then, the improved semi-implicit Additive Operator Splitting (AOS_2) scheme as proposed by Spencer and Chen (2015) was employed to solve Equations 20, 21, and 22. The details of the scheme are well explained in Spencer and Chen (2015).

Steps of the Algorithm for the Proposed Models

This algorithm shows the steps involved to implement the new proposed models to compute the solution using MATLAB software.

Algorithm 1: The $CDSS_{NEW1}$ algorithm

Step 1. The 'imread' command was used in MATLAB to input the grayscale images.

Step 2. The parameter values of α, μ, θ, and λ were set, and the distance function of $P_C(x,y)$ was calculated using the 'bwdist' command for minimization problem $CDSS_{NEW1}$.

Step 3. The parameter $u^{(0)}, n = 0$ was initialized.

Step 4. **For** $iter = 1$ to maximum iterations, *maxit* or $\frac{\left\|u^{n+1} - u^n\right\|}{\left\|u^n\right\|} \leq tol$ **do**

Calculate $c_1^{(n)}\left(u^{(n-1)}\right)$ and $c_2^{(n)}\left(u^{(n-1)}\right)$

Calculate $r_p^{(n)} = \lambda\left(\left(z - c_1^n\right)^2 - \left(z - c_2^n\right)^2\right) + \theta P_C$.

Set $\alpha^{(n)} = \left\|r_p^n\right\|_{L^\infty}$.

Calculate $f^n = \lambda r + \theta P_C + \alpha v^{'}$.

Update to $u^{(n)} \leftarrow \min_u CDSS_{NEW}(c_1^{(n)}, c_2^{(n)}, \alpha^{(n)})$ to $u^{(n+1)}$ using AOS_2 (Spencer & Chen, 2015).

end for

Step 5. $u^* \leftarrow u^{(n)}$. u^* represents the final solution.

The stopping criteria used for this model was set as the value of tolerance, $tol = 1 \times 10^{-4}$. The program would stop when $\frac{\left\|u^{n+1} - u^n\right\|}{\left\|u^n\right\|} \leq tol$ or when the program reached the maximum iterations (*maxit*), which was 5,000 iterations. This process was repeated by applying another two different distance methods $P_{CB}(x,y)$, for $CDSS_{NEW2}$, and $P_{QE}(x,y)$ for $CDSS_{NEW3}$.

EXPERIMENTAL RESULTS

In these experiments, the performance of the existing *CDSS* model was compared with $CDSS_{NEW1}$, $CDSS_{NEW2}$, and $CDSS_{NEW3}$ in segmenting a targeted object in an image. All algorithms were implemented in

MATLAB R2016a. The CPU processor used was Intel® Core TM-i5-7200U CPU @ 2.50GHz with 4 GB installed memory (RAM). The parameters were fixed at $\varepsilon = 10^{-2}, \alpha = 2, \lambda = 0.01, \mu = 1, \beta = 10^{-4}$, $\varepsilon = 0.01, tol = 10^{-4}$ and $maxit = 5000$ for all experiments, and the adjustment for the value θ was made depending on the given images. Basically, the value of θ was small for a simple image, while a larger value of θ was needed for the real image or an image with noise. For the accuracy of the segmentation result, the performance of all models was evaluated by using the Jaccard Similarity Coefficient (JSC) and Dice Similarity Coefficient (DSC) in the range of [0, 1] as follows:

$$JSC = \frac{|S_n \cap S_*|}{|S_n \cup S_*|}, \qquad DSC = 2\frac{|S_n \cap S_*|}{|S_n| + |S_*|},$$

where S_n is the segmented domain Ω_1 set and S_* is the true set of Ω_1. The test images used in this paper are listed in Figure 1.

Figure 1

Segmentation Test Images.

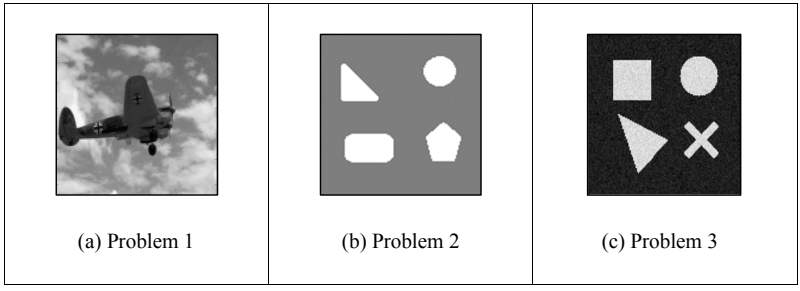

(a) Problem 1 (b) Problem 2 (c) Problem 3

Problem 1 is a real image while Problems 2 and 3 are synthetic images. The real image and benchmark for Problem 1 was obtained from Li et al. (2013). Meanwhile, Problems 2 and 3 were self-generated synthetic images. It was remarked that Problem 2 was a synthetic image without noise, while Problem 3 was a synthetic image with noise. All the test images had a size of 128 × 128 pixels. This study compared the computational speed and accuracy of segmentation for the *CDSS* model and the three modified models on all three problems. For Problems 1 and 3, the parameter was used, while the value of was used for Problem 2. Figure 2 exhibits the segmentation results of each model for Problem 1.

Figure 2

Segmentation of Problem 1 for CDSS, $CDSS_{NEW1}$, $CDSS_{NEW2}$, and $CDSS_{NEW3}$.

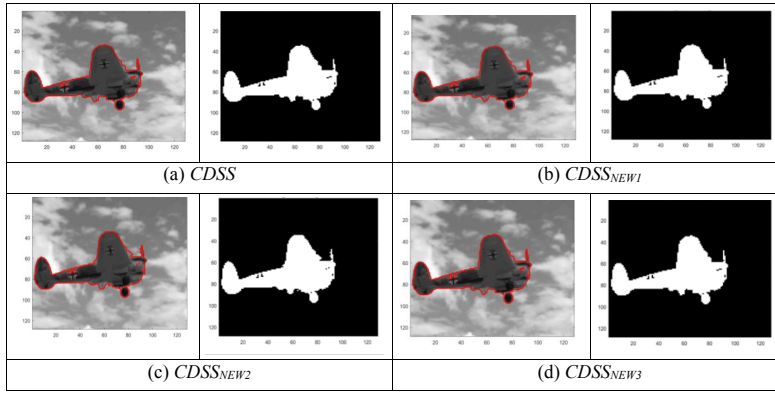

The results were in the form of curve representation (grayscale image with red line) and binary representation (black and white). All models could segment the targeted object successfully and achieve similar segmentation quality, whereby the JSC and DSC values were 0.85 and 0.92, respectively. Figure 3 demonstrates the segmentation results of each model for Problem 2.

Figure 3

Segmentation of Problem 2 for CDSS, $CDSS_{NEW1}$, $CDSS_{NEW2}$, and $CDSS_{NEW3}$.

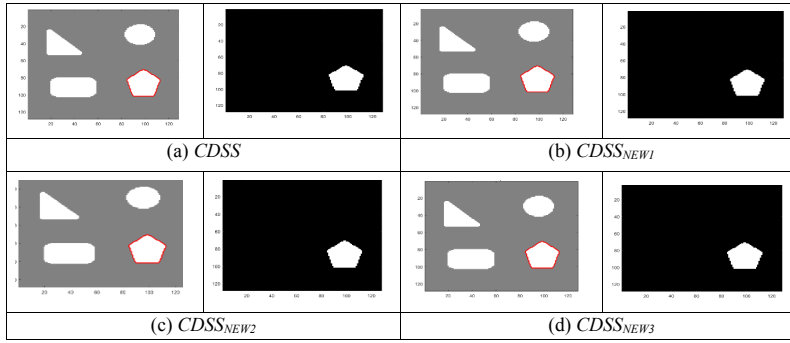

In Problem 2, the targeted object was the pentagon. The red line showed the segmentation curve while the black and white image displayed the binary representation result. All models achieved

similar segmentation quality in Problem 2 (JSC = 1, DSC = 1). Figure 4 exhibits the segmentation results of each model for Problem 3.

Figure 4

Segmentation of Problem 3 for CDSS, $CDSS_{NEW1}$, $CDSS_{NEW2}$, and $CDSS_{NEW3}$.

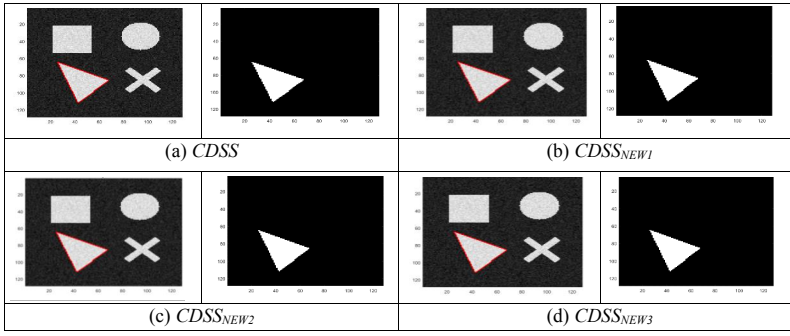

(a) *CDSS* (b) $CDSS_{NEW1}$

(c) $CDSS_{NEW2}$ (d) $CDSS_{NEW3}$

In Problem 3, the targeted object was the triangle. The grayscale image with the red line showed the segmentation curve while the black and white image demonstrated the result in binary form. The JSC values for DSS, $CDSS_{NEW1}$, $CDSS_{NEW2}$, and $CDSS_{NEW3}$ were 0.97, 0.99, 0.94, and 0.96, respectively, while the DSC values for $CDSS$, $CDSS_{NEW1}$, $CDSS_{NEW2}$, and $CDSS_{NEW3}$ were 0.98, 0.99, 0.97, and 0.98, respectively. Therefore, the $CDSS_{NEW1}$ model achieved the highest accuracy. The JSC and DSC values for all the models in segmenting all the problems are summarized in Figure 5.

Figure 5

Comparison of Segmentation Quality based on Values of JSC and DSC for All Problems.

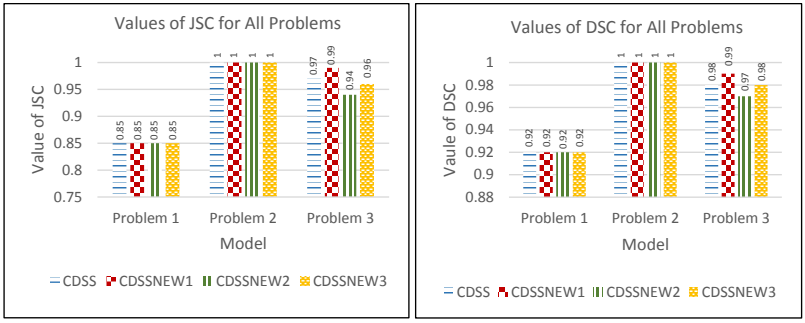

According to Figure 5, all models achieved similar segmentation quality in Problem 1 (JSC = 0.85, DSC = 0.92) and Problem 2 (JSC = 1, DSC = 1). In Problem 3, the $CDSS_{NEW1}$ model achieved the highest accuracy (JSC = 0.99, DSC = 0.99) in segmenting targeted objects, while the accuracy of segmentation results by other models showed slight variations from one another. The computational or execution time required to accomplish the segmentation task is demonstrated in Figure 6.

Figure 6

Comparison of Computational Time for All Problems.

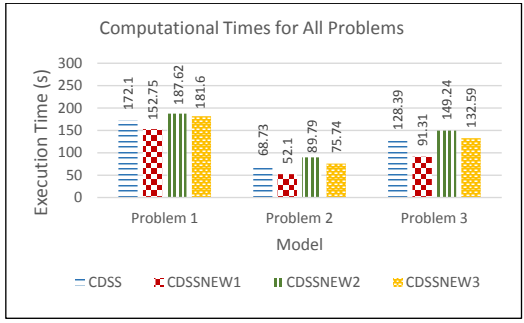

From Figure 6, the $CDSS_{NEW1}$ model with the Chessboard distance function was 11.24 percent faster than the existing model, *CDSS* in segmenting Problem 1. In Problems 2 and 3, the $CDSS_{NEW1}$ model was 24.20 percent and 28.88 percent faster than the *CDSS* model, respectively. In addition, the $CDSS_{NEW1}$ model had the fastest computational speed in segmenting targeted objects as compared to other models in all tested problems. Therefore, the findings of this study indicate that the $CDSS_{NEW1}$ model has the highest accuracy in segmentation and possesses the fastest computational time.

CONCLUSION

This study focused on segmenting specific objects selectively for grayscale images by using the selective segmentation technique. Three new models were proposed in this study, i.e., $CDSS_{NEW1,}$ $CDSS_{NEW2}$, *and* $CDSS_{NEW3}$. To minimize the functionals, the associated Euler Lagrange PDE for each model was derived. Then, the equations were solved using an Additive Operator Splitting (AOS_2) scheme proposed by Spencer and Chen (2015), computed in the MATLAB

platform. The performance of each model was analyzed based on the computational time and accuracy of segmentation results measured in terms of JSC and DSC for each test problem. The accuracy of the segmented images in Problems 1 and 2 was similar for all models. Meanwhile, in Problem 3, the $CDSS_{NEW1}$ model achieved the highest accuracy in segmenting targeted objects as compared to the other models.

The existing model, *CDSS* with Euclidean distance function, was slower than $CDSS_{NEW1}$ in terms of computational time. On the contrary, $CDSS_{NEW1}$ was faster than $CDSS_{NEW3}$ with the Quasi-Euclidean distance function and the $CDSS_{NEW2}$ model with the City Block distance function. Therefore, it can be concluded that the $CDSS_{NEW1}$ model with Chessboard distance function achieved the best performance with the fastest computational speed as compared to other models in segmenting the grayscale images selectively.

The formulation of this modified CDSS can be extended in future research to vector-valued images since these images contain richer information and have better intensity. Moreover, the minimization problem can be solved by using the multilevel method directly without using a partial differential equation. Therefore, the solution might be faster to be solved and might improve efficiency.

ACKNOWLEDGMENT

This work was supported by Geran Penyelidikan Khas (GPK) Universiti Teknologi MARA Shah Alam, grant number 600-RMC/GPK 5/3 (185/2020), 2020.

REFERENCES

Ali, H., Rada, L., & Badshah, N. (2018). Image segmentation for intensity inhomogeneity in presence of high noise. *IEEE Transactions on Image Processing*, *27*(8), 3729–3737. https://doi.org/10.1109/TIP.2018.2825101

Badshah, N., & Chen, K. (2010). Image selective segmentation under geometrical constraints using an Active Contour approach. *Commun. Comput. Phys*., *7*(4), 759–778. https://doi.org/10.4208/cicp.2009.09.026

Bastan, M., Bukhari, S. S., & Breuel, T. (2017). Active canny: Edge detection and recovery with open active contour models. *IET Image Processing*, *11*(12), 1325–1332. https://doi.org/10.1049/iet-ipr.2017.0336

Brown, E. S., Chan, T. F., & Bresson, X. (2012). Completely convex formulation of the chan-vese image segmentation model. *International Journal Computer Vision*, *98*(1), 103–121. https://doi.org/10.1007/s11263-011-0499-y

Burrows, L., Guo, W., Chen, K., & Torella, F. (2020). Reproducible kernel hilbert space based global and local image segmentation. *Inverse Problems and Imaging*, *15*(1), 1–25. http://dx.doi.org/10.3934/ipi.2020048

Caselles, V., Kimmel, R., & Sapiro. (1997). Geodesic active contour. *International Journal of Computer Vision*, *22*, 61–79. https://doi.org/10.1023/A:1007979827043

Chan, T. F., & Vese, L. A. (2001). Active contours without edges. *IEEE Transactions on Image Processing*, *10*(2), 266–277. https://doi.org/10.1109/83.902291

Chan, T. F., Esedoglu, S., & Nikolova, M. (2006). Algorithms for finding global minimizers of image segmentation and denoising models. *SIAM Journal on Applied Mathematics, 66*(5), 1632–1648. https://doi.org/10.1137/040615286

Chen, Q., Yang, X., & Petriu, E. M. (2004). Watershed segmentation for binary images with different distance transforms. In A. E. Saddik & R. Goubran (Eds.), *The 3rd IEEE International Workshop on Haptic, Audio and Visual Environments and Their Applications* (pp. 111–116). IEEE. https://doi.org/10.1109/HAVE.2004.1391891

Dobrosotskaya, J., & Guo, W. (2017). A PDE-free variational method for multi-phase image segmentation based on multiscale sparse representations. *Journal of Imaging*, *3*(3), 1–26. https://doi.org/10.3390/jimaging3030026

Felzenszwalb, P. F., & Huttenlocher, D. P. (2012). Distance transforms of sampled functions. *Theory of Computing*, *8*, 415–428. https://doi.org/10.4086/toc.2012.v008a019

Getreuer, P. (2012). Chan-vese segmentation. *Image Processing on Line*, *5*, 214–224. http://dx.doi.org/10.5201/ipol.2012.g-cv

Gout, C., Guyader, C. L., & Vese, L. (2005). Segmentation under geometrical conditions using geodesic active contours and interpolation using level set methods. *Numerical Algorithms*, *39*, 155–173. https://doi.org/10.1007/s11075-004-3627-8

Hadhoud, M., Amin, M., & Dabbour,W. (2005, December 19-21). *Detection of breast cancer tumor algorithm using*

mathematical morphology and Wavelet analysis [Paper presentation]. International Conference on Graphics, Vision and Image Processing, GVIP-05, Cairo, Egypt. http://icgst.com/conferences/paper.aspx?pid=P1150535163&confid=49

Jumaat, A. K., & Chen, K. (2020). Three-dimensional convex and selective variational image segmentation model. *Malaysian Journal of Mathematical Sciences*, *14*(3), 437–450. https://einspem.upm.edu.my/journal/fullpaper/vol14no3/7.%20Abdul%20Kadir%20Jumaat.pdf

Jumaat, A. K., & Chen, K. (2019). A reformulated convex and selective variational image segmentation model and its fast multilevel algorithm. *Numerical Mathematics Theory Methods and Applications*, *12*(2), 403–437. http://dx.doi.org/10.4208/nmtma.OA-2017-0143

Jumaat, A. K., & Chen, K. (2017). An optimization-based multilevel algorithm for variational image segmentation models. *Electronic Transactions on Numerical Analysis*, *46*, 474–504. https://etna.ricam.oeaw.ac.at/vol.46.2017/pp474-504.dir/pp474-504.pdf

Kass, M., Witkin, A., & Terzopoulos, D. (1988). Snakes: Active contour models. *International Journal of Computer Vision*, *1*(4), 321–331. https://doi.org/10.1007/BF00133570

Kaur, D., & Kaur, Y. (2014). Various image segmentation techniques: A review. *International Journal of Computer Science and Mobile Computing*, *3*(5), 809–814. https://ijcsmc.com/docs/papers/May2014/V3I5201499a84.pdf

Khan, A., & Ravi, S. (2013). Image segmentation methods: A comparative study. *International Journal of Soft Computing and Engineering*, *3*(4), 84–92. https://www.ijsce.org/wp-content/uploads/papers/v3i4/D1760093413.pdf

Khan, M. W. (2014). A survey: Image segmentation techniques. *International Journal of Future Computer and Communication*, *3*(2), 89-93. https://doi.org/ 10.7763/IJFCC.2014.V3.274

Kumar, M. J., Kumar, G. R., & Reddy, R. V. K. (2014). Review on image segmentation techniques. *International Journal of Scientific Research Engineering & Technology*, *3*(6), 993–997. http://www.ijirset.com/upload/2017/icmtest/53_A%20SURVEY%20%20ON%20IMAGE%20SEGMENTATION.pdf

Lee, Y. H., & Horng, S. J. (1996). The chessboard distance transform and the medial axis transform are interchangeable. In M. E. Kavanaugh (Ed.), *Proceeding of International Conference on Parallel Processing* (pp. 424–428). IEEE. https://doi.org/10.1109/IPPS.1996.508090

Li, W., Song, S., & Qian, X. (2011). Active Contours with selective local or global segmentation property for multiobject image. *Optical Engineering*, *50*(6), Article 067009. https://doi.org/10.1117/1.3589956

Li, H., Cai, J., Nguyen, T. N. A., & Zheng, J. (2013, July 15–19). A benchmark for semantic image segmentation [Paper presentation]. In *2013 IEEE International Conference on Multimedia and Expo (ICME)*, San Jose, CA, USA. https://doi.ieeecomputersociety.org/10.1109/ICME.2013.6607512

Mandal, S., Dean-Ben, X. L., & Razansky, D. (2016). Visual quality enhancement in optoacoustic tomography using active contour segmentation priors. *IEEE Transactions on Medical Imaging*, *35*(10), 2209–2217. https://doi.org/10.1109/TMI.2016.2553156

McInerney, T., & Terzopoulos, D. (1996). Deformable models in medical image analysis. In M. E. Kavanaugh (Ed.), *Proceedings of the Workshop on Mathematical Methods in Biomedical Image Analysis* (pp. 171–180). IEEE. https://doi.org/10.1109/MMBIA.1996.534069

Mumford, D., & Shah, J. (1989). Optimal approximations by piecewise smooth functions and associated variational problems. *Communications on Pure and Applied Mathematics*, *42*(5), 577–685. https://doi.org/10.1002/cpa.3160420503

Osher, S. J., & Sethian, J. (1988). Fronts propagating with curvature dependent speed: Algorithms based on Hamilton-Jacobi formulations. *Computational Physics*, *79*(1), 12–49. https://doi.org/10.1016/0021-9991(88)90002-2

Othman, M., Abdullah, S. L. S., Ahmad, K. A., Bakar, M. N. A., and Mansor, A. R. (2016). The fusion of edge detection and mathematical morphology algorithm for shape boundary recognition. *Journal of Information and Communication Technology,15*(1),133–144. http://e-journal.uum.edu.my/index.php/jict/article/view/8175

Perona, P., & Malik, J. (1990). Scale-space and edge detection using anisotropic diffusion. *IEEE Transactions on Pattern Analysis and Machine Intelligence*, *12*(7), 629–639. https://doi.org/10.1109/34.56205

Rada, L., & Chen, K. (2011). A new variational model with dual level set functions for selective segmentation. *Communication in Computational Phys*ics, *12*(1), 261–283. https://doi.org/10.4208/cicp.190111.210611a

Rada, L., & Chen, K. (2013). Improved selective segmentation model using one level-set. *Journal of Algorithms & Computational Technology*, *7*(4), 509–540. https://doi org/10.1260%2F1748-3018.7.4.509

Saini, S., & Arora, K. (2014). A study analysis on the different image segmentation techniques. *International Journal of Information & Computation Technology*, *4*(14), 1445–1452. http://www.ripublication.com/irph/ijict_spl/ijictv4n14spl_13.pdf

Shihab, A. I. (2000). *Fuzzy clustering algorithms and their application to medical image analysis* [Ph.D. dissertation, University of London]. Citeseer. http://citeseerx.ist.psu.edu/viewdoc/download;jsessionid=FD25B1CFA229BEFD0E5F9C0F193AD686?doi=10.1.1.116.3037&rep=rep1&type=pdf

Spencer, J., & Chen, K. (2015). A convex and selective variational model for image segmentation. *Communications on Mathematics and Sciences*, *13*(6), 1453–1472. https://doi.org/10.4310/CMS.2015.V13.N6.A5

Wei, W. B., Tan, L., Jia, M. Q., & Pan, Z. K. (2017). Normal vector projection method used for convex optimization of chan-vese model for image segmentation. *Journal of Physics: Conference Series, 787,* Article 012016. https://iopscience.iop.org/article/10.1088/1742-6596/787/1/012016

Yang, Y., & Wu, B. (2012). Convex image segmentation model based on local and global intensity fitting energy and split bregman method. *Journal of Applied Mathematics*, Article 692589. https://doi.org/10.1155/2012/692589

Yearwood, A. B. (2018). *A brief survey on variational methods for image segmentation* (Research Assignment: Chicago Referencing). ResearchGate. https://www.researchgate.net/publication/323971382_A_Brief_Survey_on_Variational_Methods_for_Image_Segmentation

Zuva, T., Olugbara, O. O., Ojo, S. O., & Ngwira, M. (2011). Image segmentation, available techniques, developments and open issues. *Canadian Journal on Image Processing and Computer Vision*, *2*(3), 20–29. https://www.researchgate.net/profile/Tranos-Zuva/publication/264854010_Image_Segmentation_Available_Techniques_Developments_and_Open_Issues/links/563b097708aeed0531dcc7a2/Image-Segmentation-Available-Techniques-Developments-and-Open-Issues.pdf